Fabrication of germanium nanodisk array by neutral beam etching with protein as etching mask

Takuya Fujii
Institute of Fluid Science, Tohoku University, 2-1-1 Katahira, Aoba-ku, Sendai, Miyagi 980-8577, Japan and Automobile R&D Center, Honda R&D Co., Ltd., 1-4-1 Chuo, Wako, Saitama 351-0193, Japan

Takeru Okada
Institute of Fluid Science, Tohoku University, 2-1-1 Katahira, Aoba-ku, Sendai, Miyagi 980-8577, Japan

Taiga Isoda
School of Fundamental Science and Technology, Keio University, 3-14-1 Hiyoshi, Kouhoku-ku, Yokohama 223-8522, Japan

Mohd Erman Syazwan
Institute of Fluid Science, Tohoku University, 2-1-1 Katahira, Aoba-ku, Sendai, Miyagi 980-8577, Japan

Mohamed-Tahar Chentir
Institute of Fluid Science, Tohoku University, 2-1-1 Katahira, Aoba-ku, Sendai, Miyagi 980-8577, Japan and Japan Science and Technology Agency (JST), CREST, Kawaguchi, Saitama 332-0012, Japan

Kohei M. Itoh
School of Fundamental Science and Technology, Keio University, 3-14-1 Hiyoshi, Kouhoku-ku, Yokohama 223-8522, Japan

Ichiro Yamashita
Graduate School of Materials Science, Nara Institute of Science and Technology, 8916-5, Takayama-cho, Ikoma, Nara 630-0192, Japan

Seiji Samukawa[a)]
Institute of Fluid Science, Tohoku University, 2-1-1 Katahira, Aoba-ku, Sendai, Miyagi 980-8577, Japan and Japan Science and Technology Agency (JST), CREST, Kawaguchi, Saitama 332-0012, Japan

(Received 2 October 2016; accepted 30 January 2017; published 16 February 2017)

A uniform 10 nm diameter Ge two-dimensional (2D) nanodisk array structure was fabricated using iron oxide cores in a 2D closed-packed array of cage shaped proteins, ferritins, as an etching mask. Thin Ge layer on Si substrate was protected by a-Si capping layer and etched, which eliminated an uncontrollable factor of Ge native oxide. The density of Ge nanodisks was as high as $5.8 \times 10^{11}\,\mathrm{cm}^{-2}$, and the center-to-center distance was estimated to be 14 nm. It was demonstrated that a quantum confinement effect can be obtained with our fabricated Ge nanodisk array by controlling the nanodisk thickness. The obtained high density Ge nanodisk is promising for Ge/Si quantum dot intermediate band solar cells and other photonics devices. © *2017 American Vacuum Society*. [http://dx.doi.org/10.1116/1.4976524]

I. INTRODUCTION

Silicon-based solar cells have a market share larger than 85% due to the abundance of the constituent elements and the advances that have been made in processing semiconductor silicon. Such cells now have a conversion efficiency that exceeds 25%, which is close to the Shockley-Queisser limit of approximately 30%,[1,2] but this is not enough to satisfy the diverse demands of commercial applications.[3] To address this issue, intermediate band solar cells (IBSCs) have been developed. The IBSCs are based on the concept that forming energy levels in the band gap, namely, mini bands, enhances photo absorption. Specifically, IBSCs absorb light whose energy is lower than that of the solar cell's base material. Indeed, carrier transition from valence band to conduction band through the intermediate band is possible, which is called two-photon-transition. This process has been demonstrated in several experiments.[4,5]

Silicon-based solar cells are viable in terms of commercial production, but there are several difficulties when producing silicon-based quantum dots (QDs) array, which includes highly precise size control due to a small Bohr radius (5 nm), the difficulty of achieving high order alignment of mini bands, problems due to complex indirect-band structure, and limitations related to growth kinetics. In contrast, germanium-based QDs have some advantages over silicon-based QDs. There are fewer restrictions on precise size control due to a large Bohr radius (24 nm), longer carrier lifetime (1 μs) due to the spatial separation of carriers,[6] and controllable band gap energy by using a $Si_{1-x}Ge_x$ alloy.[7] The band alignment between Ge and Si would provide a promising way to take advantage of the potential of IBSCs.[8] When Ge QDs are used with amorphous Si (a-Si) as a matrix material, the theoretical conversion efficiency reaches 44%,[9] so Ge/Si type-II system is one of candidates for IBSCs.

However, some technological innovations are necessary to realize Ge QD structures for IBSCs. Bottom-up processes

[a)]Electronic mail: samukawa@ifs.tohoku.ac.jp

such as S-K methods have been widely used to fabricate Ge quantum structures. However, the production cost of quantum structures using bottom-up processes is too high to adapt for large-scale industrial production of IBSCs. Another bottleneck is that they sometimes produce defects and residual stress in the structures,[10] which is problematic due to recombination of carrier, and it is impossible to eliminate the defects completely even after postannealing. Moreover, bottom-up processes cannot align quantum structures vertically or control interdot spaces horizontally. With top-down processes such as plasma etching, structural defects occur due to ultraviolet (UV) exposure.[11] It is difficult to pattern down to the sub-10 nm scale by lithography at the present time. The instability of Ge native oxide surface must also be controlled. Improvements are still required to demonstrate the essential characteristics of the Ge nanostructure itself.

In order to remove these issues, we propose a method for Ge QD fabrication that combines a neutral beam (NB) technique[12,13] with a cage-shaped protein with a nanoparticle as etching mask.[14–16] The NB technique eliminates UV light from plasma and controlling high energy ion bombardment, and biomolecule serves as nanometerically precise etching mask. In this study, we adapted the NB process to fabricate a 2D array of Ge nanodisks (Ge NDs) with neutral beam etching and carried out the optical absorption measurement.

II. EXPERIMENT

The NB system consists of a plasma chamber and a process chamber separated by a carbon electrode array with an aperture. The electrode neutralizes and collimates charged particles when plasma particles pass through it, and the aperture eliminates irradiated photons from the plasma. Under these conditions, less defective anisotropic etching becomes possible. A voltage of −100 V was applied to the top electrodes, and radio frequency (RF) 16 W was biased at the bottom electrode (aperture) to accelerate the neutral particles. A schematic illustration of this can be found in our previous paper.[17]

The fabrication of a 2D array of Ge NDs structure is schematically shown in Figs. 1(a)–1(g). First, Ge quantum well which consisted of a 10 nm thick a-Si buffer layer and a Ge layer with various thicknesses (from 2 to 8 nm) and a 3 nm thick a-Si capping layer were deposited on a quartz substrate by molecular beam epitaxy (MBE), as shown in Fig. 1(a). The deposition was performed at room temperature. After deposition, the sample was cleaned by a chemical wet process to remove organics, and then native oxide was removed by using a 2% hydrogen fluoride solution. We next performed NB oxidation (NBO) at 300 °C for 100 s with a 5 sccm oxygen flow rate, 0.11 Pa process pressure, and 13.56 MHz RF power of 500 W. Under these conditions, a 2 nm thick silicon oxide film was formed [Fig. 1(b)].[18] Ferritin was spin coated onto the sample with a rotation speed of 3000 rpm for 30 s [Fig. 1(c)]. To utilize the iron oxide core lodged in the ferritin molecule as an etching mask, the protein shell was removed by heat-treatment in a low pressure oxygen gas [Fig. 1(d)]. Temperature, oxygen gas pressure, flow rate, and treatment time were 280 °C, 32 Pa, 100 sccm, and 30 min, respectively. We also removed the surface Si oxide (NBO) layer by dry etching process using a nitrogen trifluoride gas/hydrogen radical treatment (NF_3 treatment),[19–22] as shown in Fig. 1(e). NF_3 treatment was performed with a 70 sccm NF_3 flow rate and a 10 sccm hydrogen flow rate for 20 min, and then, the wafer was annealed at 100 °C with a 38 sccm hydrogen flow rate for 15 min. NB etching was performed using 40 sccm of chlorine gas with 16 W of RF bias power at the bottom electrode at 30 °C without breaking the vacuum [Fig. 1(f)]. Finally, a 2D array of Ge NDs structure was obtained by removing the iron oxide cores using a hydrochloric acid solution [Fig. 1(g)].

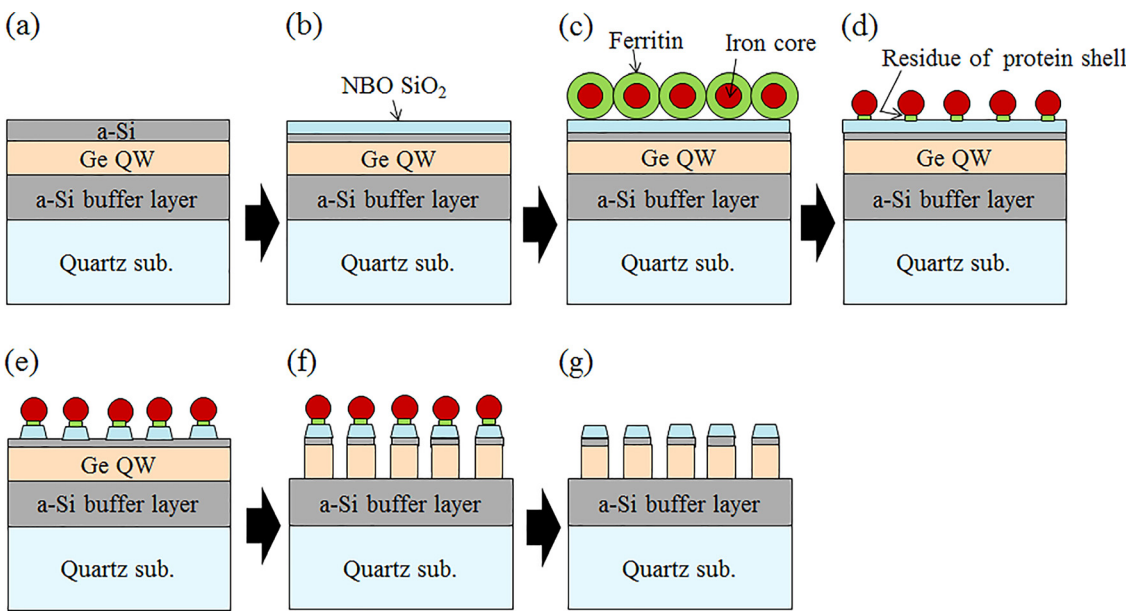

FIG. 1. (Color online) Process flow of Ge ND fabrication. (a) Deposition of Si/Ge layers (Ge quantum well), (b) NBO, (c) arrangement of 2D array of ferritin molecules, (d) removal of ferritin protein shells, (e) removal of Si oxide layer by NF_3 treatment, (f) neutral beam etching, and (g) removal of iron oxide cores.

Although, in principle, our neutral beam process could apply to all processes of fabrication of nanodisks, we did not use it for the protein removal process and the SiO_2 removal process. The reason why we did not use it is as follows.

As for the protein removal process, we have tried using oxygen neutral beam. Although it could completely remove the protein, it resulted in the lower density of ferritin after the process compared with the case of thermal annealing in oxygen gas. Therefore, we did not use the oxygen neutral beam for the protein removal process.

As for the SiO_2 removal process, flourin neutral beam could etch SiO_2 layer. However, it could also etch and shrink iron cores which works as an etching mask. In this case, it might make difficult to etch Ge sufficiently. On the other hand, NF_3 treatment can etch only SiO_2 layer selectively. Therefore, we used NF_3 treatment for the SiO_2 removal process.

The surface morphology of the sample was observed with a scanning electron microscope (SEM, Hitachi 5400), and the optical absorption was measured by UV-Vis-NIR spectroscopy (JASCO V-670).

III. RESULTS AND DISCUSSION

A. Ferritin arrangement on Si-capped Ge

The first requirement for fabricating the Ge ND array is to form a 2D array of ferritin with iron oxide core on the substrate. After protein shell elimination, the array of iron oxide cores works as an etching mask. Our preceding work showed that a 2D array of ferritin arrangement on silicon dioxide surface can be achieved by spin-coating technique where balance of electrostatic force and hydrophilic interaction among ferritins and a substrate plays the important role.[12,23] However, ferritin adsorption on native Ge surface by spin-coating could not produce high density 2D arrays. The surface was not fully covered, and vacancies were observed [Fig. 2(a)]. This may be due to the quick Ge surface oxidization when exposed to air and high solubility of Ge oxide when subjected to ferritin aqueous solution. These might make the stable balance difficult among ferritins and the substrate during the 2D array formation, which leads to poor 2D arrangement. The results indicated that the Ge surface could not be used without being protected.

We deposited Si on the Ge surface in vacuum as a protection layer and performed 2D ferritin array formation. The surface was fully covered with ferritin, as shown in Fig. 2(b). Ferritin arrangement is closed packed. The average distance is 12.4 ± 2.4 nm. This is the same with known ferritin diameter (12.5 nm). The density is estimated as $7 \times 10^{11}\,\mathrm{cm}^{-2}$. This value is a nearly geometric limitation of 2D packing of ferritin. We can arrange ferritin with high density to fabricate Ge ND in the same manner as we discussed previously.[24,25]

The deposited Si layer was expected to protect Ge from oxidization. After Si had been deposited and oxidized by NBO, XPS analysis was performed. Figure 3 shows the results. In the Si 2p region, two peaks appeared at 100 and 104 eV that were attributed to the Si and its oxide, respectively. In contrast, in the Ge 3d region, no specific subpeaks

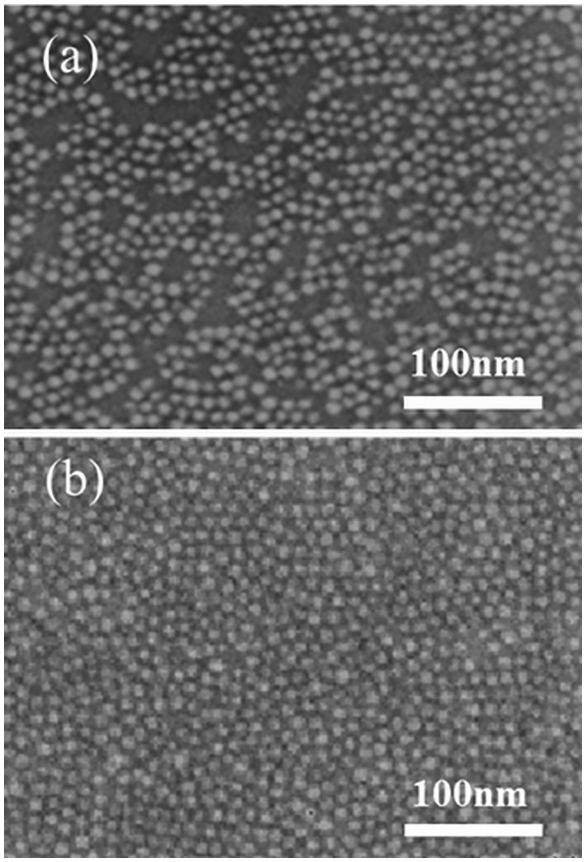

FIG. 2. SEM images of ferritin arrangement: (a) Ge native oxide sample and (b) on Si-capped Ge sample. White dots represent the iron oxide cores and protein shells were not visualized due to low density.

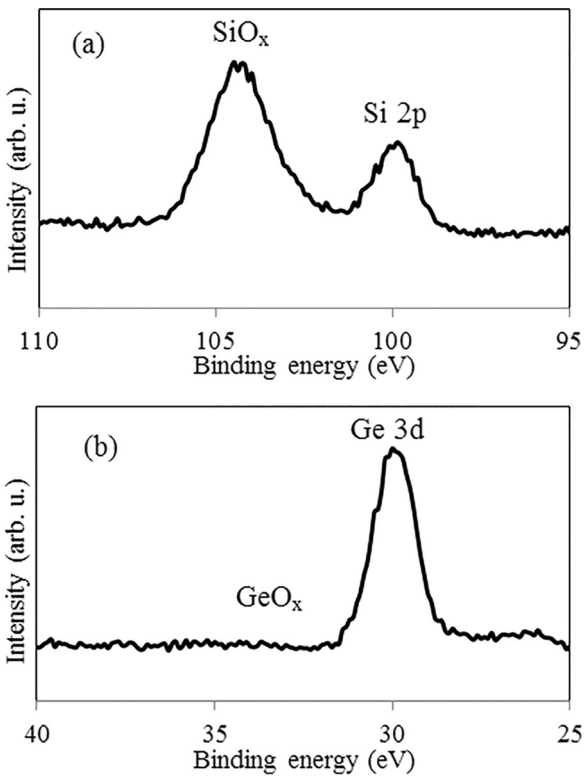

FIG. 3. XPS spectra of Si-capped Ge after NBO. (a) Si 2p and (b) Ge 3d region.

appeared. This means that the Ge layer was not oxidized during the deposition process, and it remained unoxidized even after the Si-capping layer was NB oxidized and then exposed to air.

B. Ge ND fabrication by neutral beam etching

To utilize the iron oxide core contained in the ferritin molecules as an etching mask, it was necessary to remove the protein shell. A rapid thermal annealing (RTA) process was performed for the protein removal. Since long processing at high temperature should be avoided to prevent interdiffusion between Ge and Si or aggregation of the iron oxide cores, annealing was performed at 280 °C under low oxygen gas pressure of 32 Pa. We expected the protein to evaporate at a relatively low temperature under these conditions. The protein elimination was investigated by XPS. Because protein contains nitrogen, the N1s peak intensity was measured and plotted as a function of annealing time (Fig. 4). The N1s intensity decreased with an increase in heat-treatment time and disappeared after 45 min, indicating that the ferritin protein shell was completely removed. We also observed the core distribution state using SEM. The inset images in Fig. 4 show iron oxide cores after annealing (a) for 45 min and (b) for 30 min. As shown in the SEM images, in the case of the 30 min of oxygen annealing, the iron oxide cores were close packed with the density at $7 \times 10^{11}\,\mathrm{cm}^{-2}$ as is the same with before heat-treatment. On the other hand, there are some core aggregates and fairly large area where the SiO_2 surface was seen after 45 min of oxygen annealing. As shown in Fig. 5, the protein shell portion just underneath the core might anchor the core, behaving like glue, during the protein elimination process. After the protein shell disappeared, iron oxide core that positioned weakly on the substrate starts to aggregate, which is normal for bare iron oxide nanoparticles in heat-treatments. Therefore, it can be concluded that the 30 min of oxygen annealing is optimum.

We then performed the NB technique to etch this sample using pure chlorine gas for plasma generation. After removing the Si oxide layer by NF_3 treatment as described above, we obtained a Ge ND structure by performing the NB

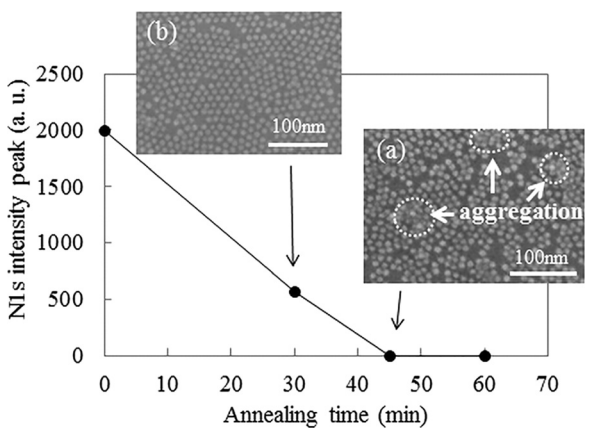

FIG. 4. N1 intensity dependence on annealing time obtained from XPS spectrum and (inset) SEM images of iron oxide cores after annealing (a) for 45 min and (b) for 30 min.

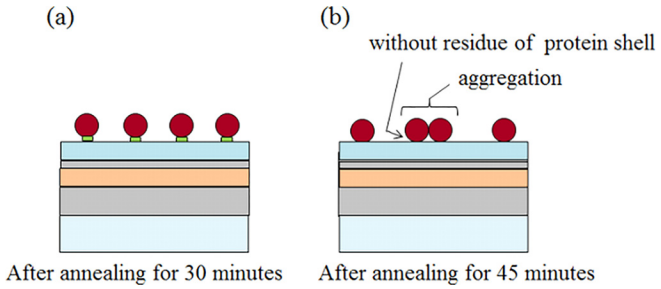

FIG. 5. (Color online) Schematic illustration of the removal process of protein shell (a) after annealing for 30 min (with residue of protein shell) and (b) after annealing for 45 min (without residue of protein shell).

etching process. SEM image is shown in Fig. 6. In Fig. 6, Ge NDs appear as separately located white dots. The diameter and center-to-center distance between dots are estimated to be 10 nm and 14.2 ± 3.3 nm, respectively. The density of isolated dots is $5.8 \times 10^{11}\,\mathrm{cm}^{-2}$. However, some vacancies and aggregations can be observed after etching. There are two possible causes of the decrease in the density after etching. First, the volume of the ferritin is reduced by the protein shell removal process and the interspace, where the iron oxide cores can move, increased about 50% from geometrical point of view, as shown in Fig. 7(a). In this situation, the iron oxide cores have possibility to aggregate or detach during etching process. Second, the iron oxide cores do not strongly adhere to the Si surface due to the relatively lower annealing temperature (280 °C) compared with preceding studies (400–500 °C).[14–16] Some of the weakly positioned cores were detached and did not work as nanomask, as shown in Fig. 7(b).

C. Optical characteristics

One of the key factors for QD solar cell is the bandgap energy (E_g). In order to investigate the bandgap energy of Ge ND, we carried out optical absorption measurement using UV-Vis-NIR spectroscopy. The absorption coefficient at each photon energy was determined by the following equation:

$$\alpha = (1/d)\ln[T/(1-R)], \tag{1}$$

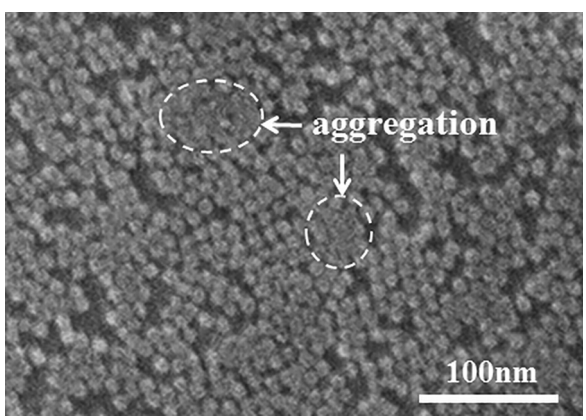

FIG. 6. SEM image of Ge ND. Picture was taken from top.

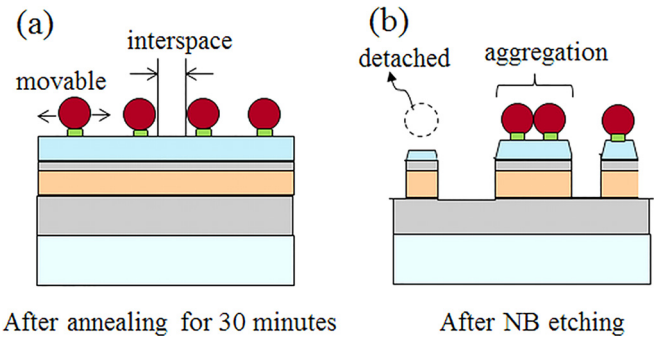

FIG. 7. (Color online) Schematic illustration of the fabrication of Ge ND with (a) after annealing for 30 min and (b) after etching.

where α is the absorption coefficient, d is the ND thickness, and R and T are the measured reflectance and transmittance, respectively.

To determine the optical bandgap of the Ge ND, we used the Tauc's formula (so-called Tauc plot)[26–28] which is derived from the equation of the absorption coefficient[29] [Eq. (2)]

$$(\alpha h\nu)^{1/2} = A(h\nu - E_g), \tag{2}$$

where h is Planck's constant, ν is the frequency, A is a constant, and E_g is the optical band gap energy. We plotted $(\alpha h\nu)^{1/2}$ versus photon energy ($h\nu$), and the band gap energy was estimated by linear fitting at the band edge as shown by dashed lines in Fig. 8(a). In Fig. 8(a), we can see a linear region in the photon energy range of 2.3–2.8 eV that indicates the onset of absorption. Therefore, extrapolating this linear region to the abscissa of photon energy shows the optical band gap energy (E_g) of the Ge NDs. In the photon energy range above 2.8 eV, another linear region where the slopes are a little steeper can be observed. It is considered to be indicative of the absorption of amorphous Si (a-Si) as a capping and a buffer layer. The absorption in the photon energy range below 2.3 eV is considered to be indicative of a so-called urbach tail[30,31] associated with the crystalline lattice disordering.

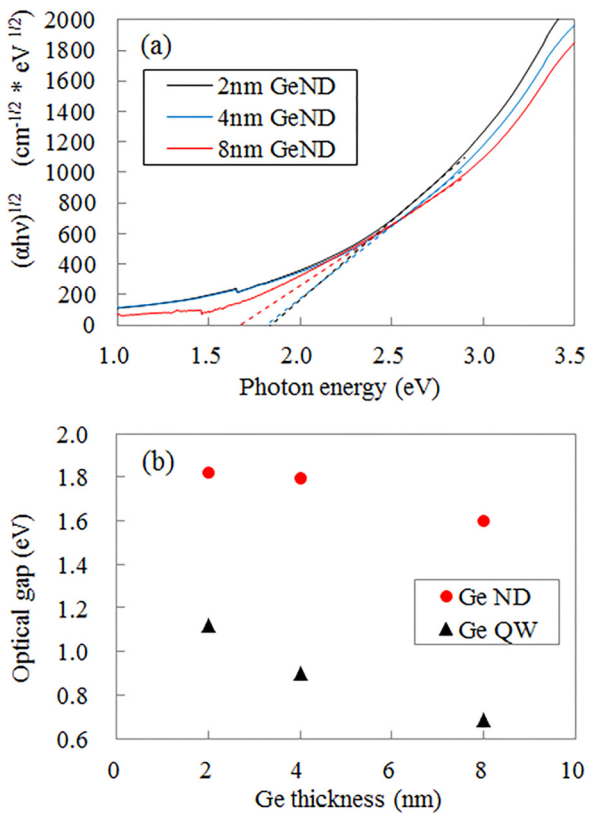

FIG. 8. (Color online) (a) Tauc plot of etched sample with various Ge thicknesses. (b) Band gap dependence of QW and ND on Ge thickness.

If the size of the nanostructure such as a quantum dot is smaller than the Bohr radius (e.g., Si < 5 nm, Ge < 24 nm), the confinement of the movement of excitons occurs and its energy levels become discrete. Then, it results in the increase of the band gap energy with the decrease in the size of the nanostructure. This effect is known as quantum confinement effect.[32] To check this effect, we estimated the band gap energy of Ge ND with various thicknesses. We also estimated the band gap energy of Ge quantum well (Ge QW) for comparison. As shown in Fig. 8(b), the band gap energy of Ge ND is increased with decreasing ND thickness and is higher than that of Ge QW. These results demonstrate that a quantum confinement effect can be obtained with our fabricated Ge ND array by controlling the ND thickness.

In this paper, we have shown a quantum effect of single layer of Ge NDs 2D packed structure fabricated by top down process. The volume of NDs was not enough to detect the overlap of wavefunction in the in-plane direction. However, the problem can be solved by fabricating the stack layer before NB etching process to gain optical response. Our proposal of the fabrication method has an advantage in the stack layer because wavefunction coupling in both vertical and in-plane directions can be expected, which realize key issue to fabricate IBSC using the Si/Ge system.

IV. SUMMARY AND CONCLUSIONS

We fabricated high-density ($5.8 \times 10^{11}\,cm^{-2}$) Ge NDs with the diameter of 10 nm by neutral beam etching with ferritin containing nanoparticle as the etching mask. We have shown that there were two key-factors for 2D packing of ferritin. The first one was the elimination of uncontrollable factor of Ge native oxide surface layer by depositing the Si-capping layer on the Ge surface, and the other one was the optimization of heat-treatment process for the protein removal. In our process, changing the Ge ND thickness enables the band gap energy. This makes it possible to modulate the band gap of a Ge quantum structure with high accuracy, and our method shows great potential for developing novel Ge-based intermediate band solar cells and other photonics devices.

[1]W. Shockley and H. J. Queisser, J. Appl. Phys. **32**, 510 (1961).
[2]M. A. Green, K. Emery, Y. Hishikawa, W. Warta, and E. A. Dunlop, Prog. Photovoltaics **23**, 1 (2015).
[3]T. Soga, NPG Asia Mater. **2**, 96 (2010).
[4]A. Marti, E. Antolin, C. R. Stanley, C. D. Farmer, N. Lopez, P. Dıaz, E. Canovas, P. G. Linares, and A. Luque, Phys. Rev. Lett. **97**, 247701 (2006).

[5]Y. Okada, T. Morioka, K. Yoshida, R. Oshima, Y. Shoji, T. Inoue, and T. Kita, J. Appl. Phys. **109**, 024301 (2011).
[6]S. Fukatsu, H. Sunamura, Y. Shiraki, and S. Komiyama, Appl. Phys. Lett. **71**, 258 (1997).
[7]Y. Shiraki and A. Sakai, Surf. Sci. Rep. **59**, 153 (2005).
[8]A. M. Kechiantz, L. M. Kocharyan, and H. M. Kechiyants, Nanotechnology **18**, 405401 (2007).
[9]W. Hu, M. M. Rahman, M. Y. Lee, Y. Li, and S. Samukawa, J. Appl. Phys. **114**, 124509 (2013).
[10]J. Drucker, IEEE J. Quantum Electron. **38**, 975 (2002).
[11]T. Yunogami, T. Mizutani, K. Suzuki, and S. Nishimatsu, Jpn. J. Appl. Phys., Part 1 **28**, 2172 (1989).
[12]C. H. Huang, M. Igarashi, M. Wone, Y. Uraoka, T. Fuyuki, M. Takeguchi, I. Yamashita, and S. Samukawa, Jpn. J. Appl. Phys., Part 1 **48**, 04C187 (2009).
[13]C. H. Huang, X. Y. Wang, M. Igarashi, A. Murayama, Y. Okada, I. Yamashita, and S. Samukawa, Nanotechnology **22**, 105301 (2011).
[14]I. Yamashita, Thin Solid Films **393**, 12 (2001).
[15]S. Yoshii, K. Yamada, N. Matsukawa, and I. Yamashita, Jpn. J. Appl. Phys., Part 1 **44**, 1518 (2005).
[16]I. Yamashita, K. Iwahori, and S. Kumagai, Biochim. Biophys. Acta **1800**, 846 (2010).
[17]T. Kubota *et al.*, J. Vac. Sci. Technol., B **25**, 760 (2007).
[18]A. Wada, K. Endo, M. Masahara, C. H. Huang, and S. Samukawa, Appl. Phys. Lett. **98**, 203111 (2011).
[19]H. Nishino, N. Hayasaka, and H. Okano, J. Appl. Phys. **74**, 1345 (1993).
[20]H. Ogawa, T. Arai, M. Yanagisawa, T. Ichiki, and Y. Horiike, Jpn. J. Appl. Phys., Part 1 **41**, 5349 (2002).
[21]J. Kikuchi, M. Iga, H. Ogawa, S. Fujimura, and H. Yano, Jpn. J. Appl. Phys., Part 1 **33**, 2207 (1994).
[22]S. Samukawa *et al.*, Appl. Phys. Express **1**, 074002 (2008).
[23]T. Matsui, N. Matsukawa, K. Iwahori, K. Sano, K. Shiba, and I. Yamashita, Langmuir **23**, 1615 (2007).
[24]M. F. Budiman *et al.*, Nanotechnology **23**, 065302 (2012).
[25]M. Igarashi, R. Tsukamoto, C. H. Huang, I. Yamashita, and S. Samukawa, Appl. Phys. Express **4**, 015202 (2011).
[26]J. Tauc, R. Grigorovici, and A. Vancu, Phys. Status Solidi B **15**, 627 (1966).
[27]J. Tauc, A. Menth, and D. L. Wood, Phys. Rev. Lett. **25**, 749 (1970).
[28]J. Tauc, *Amorphous and Liquid Semiconductors*, edited by J. Tauc (Plenum, New York, 1974), Chap. 4.
[29]P. Y. Yu and M. Cardona, *Fundamentals of Semiconductors: Physics and Materials Properties* (Springer-Verlag, Berlin, 1996), Chap. 6.
[30]F. Urbach, Phys. Rev. **92**, 1324 (1953).
[31]J. Tauc and A. Menth, J. Non-Cryst. Solids **8–10**, 569 (1972).
[32]R. Rossetti and L. Brus, J. Phys. Chem. **86**, 4470 (1982).